AGU ADVANCING EARTH AND SPACE SCIENCES

Geophysical Research Letters

RESEARCH LETTER

10.1029/2026GL123139

Key Points:

- Extreme vapor pressure deficit (EVPD) has increased significantly over the past few decades, both in frequency and intensity
- Climate change-driven increases in the frequency and intensity of extremely high temperatures are the primary drivers behind EVPD increases
- EVPD is expected to continue increasing to 7–15 standard deviations above the historical values by the end of the century

Supporting Information:

Supporting Information may be found in the online version of this article.

Correspondence to:

A. Chang,
achang1029@g.ucla.edu

Citation:

Chang, A., Zhuang, Y., Fu, R., Worden, J. R., Gu, Y., Costa, M. H., et al. (2026). Rapid increases in heat-driven extreme moisture demand in the Southern Amazon. *Geophysical Research Letters*, *53*, e2026GL123139. https://doi.org/10.1029/2026GL123139

Received 9 APR 2026
Accepted 28 JUL 2026

Author Contributions:

Conceptualization: Alex Chang, Rong Fu
Data curation: Alex Chang, Yizhou Zhuang
Formal analysis: Alex Chang, Yizhou Zhuang, Rong Fu
Funding acquisition: Rong Fu
Investigation: Alex Chang, Rong Fu
Methodology: Alex Chang, Yizhou Zhuang, Rong Fu
Project administration: Alex Chang, Rong Fu
Resources: Yizhou Zhuang, Rong Fu
Software: Alex Chang, Yizhou Zhuang
Supervision: Yizhou Zhuang, Rong Fu

Rapid Increases in Heat-Driven Extreme Moisture Demand in the Southern Amazon

Alex Chang[1], Yizhou Zhuang[1,2], Rong Fu[1,3], John R. Worden[1], Yu Gu[3], Marcos Heil Costa[4], Kaiyu Guan[5], Jiaying Zhang[6], Xiao-Peng Song[7], and Jonathan H. Jiang[3,8]

[1]Department of Atmospheric and Oceanic Sciences, University of California, Los Angeles, Los Angeles, CA, USA, [2]Department of Geography, Hong Kong Baptist University, Kowloon, Hong Kong, [3]Joint Institute for Regional Earth System Science and Engineering, University of California, Los Angeles, Los Angeles, CA, USA, [4]Department of Agricultural Engineering, The Federal University of Viçosa, Viçosa, Brazil, [5]Institute for Sustainability, Energy, and Environment, University of Illinois Urbana-Champaign, Champaign, IL, USA, [6]Department of Mathematics, College of Sciences, China Jiliang University, Hangzhou, China, [7]Department of Geographical Sciences, University of Maryland, College Park, MD, USA, [8]Beacon in the Cosmos, LLC, Pasadena, CA, USA

Abstract Extreme vapor pressure deficit (EVPD), representing the 5% hottest and driest surface air conditions, has risen rapidly over the Southern Amazon during the dry season, especially over forested areas. Its frequency has increased by 7 ± 1.5% (or 11 more dry season days) per decade, and its intensity has increased at rates faster than that of mean vapor pressure deficit (VPD), primarily due to rising extreme surface temperatures. Our observation-based attribution analysis shows that anthropogenic forcings are primarily responsible for 93% and 64% of the increases in EVPD frequency and intensity, respectively. Under a scenario close to current greenhouse gas emission trends (SSP 2–4.5), climate models project that dry season EVPD intensities will reach 7–15 standard deviations above climatological levels by the end of the century, substantially increasing the risks of extreme weather conditions conducive to wildfires in the Southern Amazon.

Plain Language Summary This study shows that rising extreme surface temperatures have substantially intensified extreme vapor pressure deficit (EVPD), an indicator of extremely hot and dry surface air, over the past few decades, particularly in the Southern Amazon during the dry season. These changes have increased the likelihood of atmospheric conditions associated with higher risks of ecosystem stress and wildfires. If emissions remain close to their current trajectory, climate models project that dry-season EVPD will rise far beyond the range of normal values seen today, substantially increasing wildfire risks in the Southern Amazon by the end of the century. These risks can be significantly reduced under the "sustainability" emission pathway.

1. Introduction

The Amazon rainforest is an important regulator of global carbon fluxes and has been a carbon sink for the global atmosphere. However, this sink has declined by nearly 50% from 1984 to 2014 (Gatti et al., 2021; Hubau et al., 2020). Furthermore, the Amazon has become a carbon source during extreme droughts in recent decades, especially over the southeastern Amazon (Yang et al., 2018). In addition to climate impacts, more frequent wildfires (Basso et al., 2023; Clarke et al., 2022) and land-use changes (Crivelari-Costa et al., 2023) also weaken this carbon sink.

Vapor Pressure Deficit (VPD) is a widely used indicator of atmospheric moisture demand. It is defined as the difference between saturation vapor pressure (e_s), which represents the atmosphere's maximum water vapor capacity, and actual vapor pressure (e_a), which represents the moisture content in the atmosphere. High VPD indicates low atmospheric relative humidity, which is conducive to increased vegetation water stress and wildfire risks. Following the Clausius-Clapeyron relationship, warmer temperatures exponentially increase e_s, and when e_a does not increase at the same rate as that of e_s, VPD increases as a result. VPD has been increasing in the Amazon in recent decades, especially during the dry season in the Southern Amazon (Jain et al., 2021). Barkhordarian et al. (2019) showed that increases in VPD are primarily due to decreases in surface humidity instead of increases in surface temperatures, the latter of which is mainly driven by increased greenhouse gases, natural variability in precipitation, and deforestation.

Validation: Alex Chang, Yizhou Zhuang, Rong Fu
Visualization: Alex Chang, Rong Fu
Writing – original draft: Alex Chang
Writing – review & editing: Alex Chang, Yizhou Zhuang, Rong Fu, John R. Worden, Yu Gu, Marcos Heil Costa, Kaiyu Guan, Jiaying Zhang, Xiao-Peng Song, Jonathan H. Jiang

Extreme VPD (EVPD), commonly represented by the 95th percentile of VPD values for a climatological period, indicates extremely hot and/or dry surface air relative to its climatology. Increases in EVPD are conducive to extensive ecological and agricultural impacts, including but not limited to reduced vegetation growth (Grossiord et al., 2020; Sancho-Knapik et al., 2022), higher vegetation mortality rates (Will et al., 2013), reduced crop yields (Leite-Filho et al., 2021), increased risk of plant hydraulic failure (Novick et al., 2024), and increased frequency of wildfires and burned areas (Flores et al., 2024; Novick et al., 2024). EVPD is often the result of extreme weather that arises from natural climate variability. Thus, EVPD can be more influenced by natural climate variability than seasonal mean VPD is. However, it remains unclear how EVPD has changed, whether EVPD changes have been driven by changes in extreme surface temperature or humidity, and whether it is mainly driven by natural climate variability or anthropogenic forcing.

Because climate models have shown persistent dry biases over the Amazon (Joetzjer et al., 2013; Li & Fu, 2006; Stouffer et al., 2017; Yin et al., 2014), we use a combined observation-based attribution and climate model-based attribution method to clarify the following research questions:

- Are the observed changes in EVPD in the Southern Amazon primarily due to changes in extreme temperatures or extreme humidity?
- Are the observed changes in EVPD in the Southern Amazon primarily due to anthropogenically forced climate change or natural variability?
- Will the observed changes in EVPD in the Southern Amazon continue in the future? What kinds of future impacts will this have in the Southern Amazon?

2. Materials and Methods

2.1. Reanalysis Data

The European Center for Medium-Range Weather Forecasts Reanalysis Version 5 (ERA5) is used in this study. Further details about ERA5 can be found in Hersbach et al. (2020). Details about ERA5 relevant to this study are available in Supporting Information S1.

2.2. Climate Model Data and Bias Corrections

For the future projections in this study, multiple models' ensembles from the Coupled Model Intercomparison Project version 6 (CMIP6) are used (Eyring et al., 2016). The details are highlighted in Supporting Information S1. All of the CMIP6 data are bias-corrected using a statistical method called quantile delta mapping (QDM). More details about this method are also provided in Supporting Information S1. All data is based on surface-level measurements unless otherwise specified. We use two different Shared Socioeconomic Pathway (SSP) scenarios for the future simulations part of this study: SSP 1-2.6 and SSP 2-4.5.

To establish a baseline, we compare historical simulations from the CMIP6 multi-model ensemble with our best estimated climate records for the Amazon, the ERA5, as our observational reference (Hersbach et al., 2020). For simplicity, we refer to the ERA5 reanalysis as "observations." EVPD intensity values and the likelihood of mean VPD exceeding 25 hPa are computed using daily CMIP6 multi-model outputs and daily ERA5 data. These are then averaged over the dry season at each spatial location within the Southern Amazon. 25 hPa was chosen because when VPD exceeds 25 hPa over tropical moist biomes such as the Southern Amazon, the risk of wildfires increases (Clarke et al., 2022) and vegetation begins to experience water stresses (Grossiord et al., 2020).

We chose the reference period of 1979–2000 for this study to represent the CMIP6 historical baseline and verified the stationarity and Gaussian distributions of the EVPD intensity trends through a Kolmogorov-Smirnov 2-sample test between the 1979–1989 and 1990–2000 distributions, as shown in Figure S1 in Supporting Information S1.

The CMIP6 historical simulations represent a range of possible climate trajectories arising from internal variability within the coupled Earth system and from structural uncertainties across different climate models. The ensemble mean of multi-model simulations approximates the forced climate response, averaging out internal variability and much of the random model uncertainty. Thus, it provides an estimate of the most likely climate trajectory under a given climate forcing scenario. The CMIP6 natural forcing-only simulations are similar except that they only account for natural forcings (e.g., solar, volcanic) in their simulations. These are used to justify the use of the analog method as described below.

2.3. Definition of EVPD, Extreme e_s, and Extreme e_a Frequency and Intensity

EVPD frequency is defined as the percentage of dry season days each year in which VPD anomalies exceeded the 95th percentile of 1979–2000 VPD anomalies. To determine how the changes in extremely high surface temperatures and low humidity have contributed to increases in EVPD frequency, we define extreme e_s frequency as when only e_s exceeds its 95th percentile values of 1979–2000 during the days when the EVPD threshold was exceeded (when e_a is not below the 5th percentile). Similarly, we define extreme e_a frequency as when only e_a values are below its 5th percentile of 1979–2000 values during the days when the EVPD threshold was exceeded (when e_s is not above the 95th percentile). As these are mutually exclusive definitions, we define extreme e_s and extreme e_a co-occurrence as when both variables exceed their respective extreme thresholds simultaneously. Additionally, because it is possible for EVPD to occur without either extreme e_s or e_a occurring in some cases, we define a similar frequency metric to assess the trends in such occurrences.

EVPD intensity is defined as the 95th percentile of VPD anomalies (relative to 1979–2000) during the dry season each year. Extreme e_s intensity is defined similarly, and extreme e_a intensity is also defined similarly but with the 5th percentile instead.

2.4. Multivariate Ensemble Constructed Flow Analog

Given the 45-year observational record, the observed trends are influenced by interannual and multidecadal natural climate variability (e.g., ENSO, AMO). Natural variability drives synoptic-scale atmospheric circulation patterns that strongly modulate VPD, dominating over more subtle anthropogenic influences on the atmospheric circulation at daily timescales (Deser et al., 2012; Hawkins & Sutton, 2012). To isolate this natural variability, we utilize an observation-based ensemble constructed flow analog approach to estimate the expected VPD values associated with daily atmospheric circulation patterns and their variations from interannual to multidecadal time scales (Lehner et al., 2018; Yiou, 2014; Yiou et al., 2007; Zhuang et al., 2021).

The analog EVPD for a given weather pattern is derived from the observed VPD values averaged over a suite of similar weather patterns during the baseline period (1979–2000) (Materials and Methods). It represents the EVPD expected for a given atmospheric circulation pattern, including its direct dynamical and thermodynamical influences, as well as associated feedbacks such as land–surface and cloud–radiation feedbacks induced by that circulation pattern. In the absence of climate change, the influence of a circulation pattern on EVPD would remain the same as its analog value throughout the analysis period apart from random variability. Because daily atmospheric circulation patterns are primarily influenced by natural climate variability, we use the analog EVPD as an approximation of the EVPD driven by natural climate variability without the influence of climate change. The residual EVPD, defined as the difference between the observed and analog EVPD, is then used as an approximation of the EVPD attributable to climate change. Similarly, the analog and residual e_s and e_a are used as approximations of e_s and e_a associated with natural climate variability and climate change, respectively.

Because the Amazon is in a humid tropical climate (which is very different from mid-latitude and/or subtropical climates focused on in the previous studies), we train a multivariate flow analog over a domain capturing the large-scale Southern Amazon circulation (85°W to 30°W, 15°N to 35°S). Further details on how the analog is trained and optimized are available in Supporting Information S1.

3. Results

3.1. Observed EVPD Trends and Causes

Our analysis focuses on the Southern Amazon (65°W to 50°W, and 5°S to 17°S) during the dry season (June–October), where and when the largest increases in seasonal mean VPD have been observed (Barkhordarian et al., 2019). This region has varying degrees of tree cover percentage (Figure S2 in Supporting Information S1), but the northern and western areas are generally more forested than the southern and eastern areas of the region.

Figure 1 compares changes in dry season EVPD intensity trends with those of dry season mean VPD intensity in South America from 1979 to 2023. As with mean VPD intensity (Figure 1a and Figure S3a in Supporting

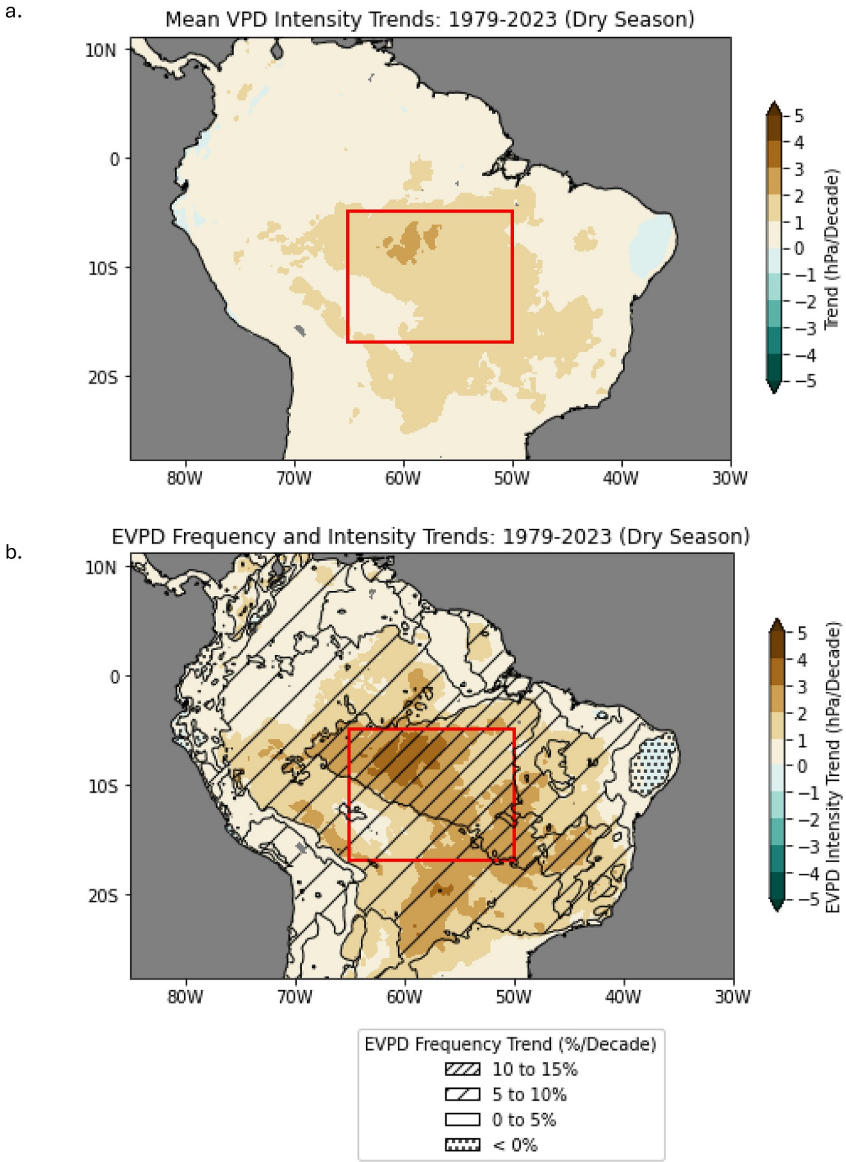

Figure 1. (a) Averaged VPD intensity trends from 1979 to 2023 across tropical South America during the dry season, and (b) averaged EVPD frequency and intensity trends during the same time period and region. Hatched areas indicate EVPD frequency trends, while colored areas indicate EVPD intensity trends.

Information S1), changes in EVPD intensity are also greater in the Southern Amazon than in other areas of South America, and during the dry season than in other seasons (Figure 1b and Figure S3b in Supporting Information S1). Within the Southern Amazon, mean VPD intensity during the dry season increased by up to 3 hPa per decade (Figure 1a). By comparison, EVPD intensity during the dry season increased by up to 4 hPa per decade in most of the Southern Amazon (Figure 1b), which is faster than that of mean VPD in almost all areas of the Southern Amazon. The greatest EVPD intensity increases occur in the more heavily forested northwestern areas (Figure S2 in Supporting Information S1), and EVPD intensity increases at slower rates in the moderately forested southwestern and northeastern parts of the Southern Amazon. In addition, EVPD frequency has been increasing at an alarming rate of more than 10% per decade over much of the Southern Amazon, and only in the moderately forested areas of the southwestern Southern Amazon does EVPD frequency increase at less than 10% per decade. Despite the spatial variations in EVPD frequency and intensity trends, they indicate larger-scale increases in evaporative demand over the Southern Amazon as a whole.

10.1029/2026GL123139

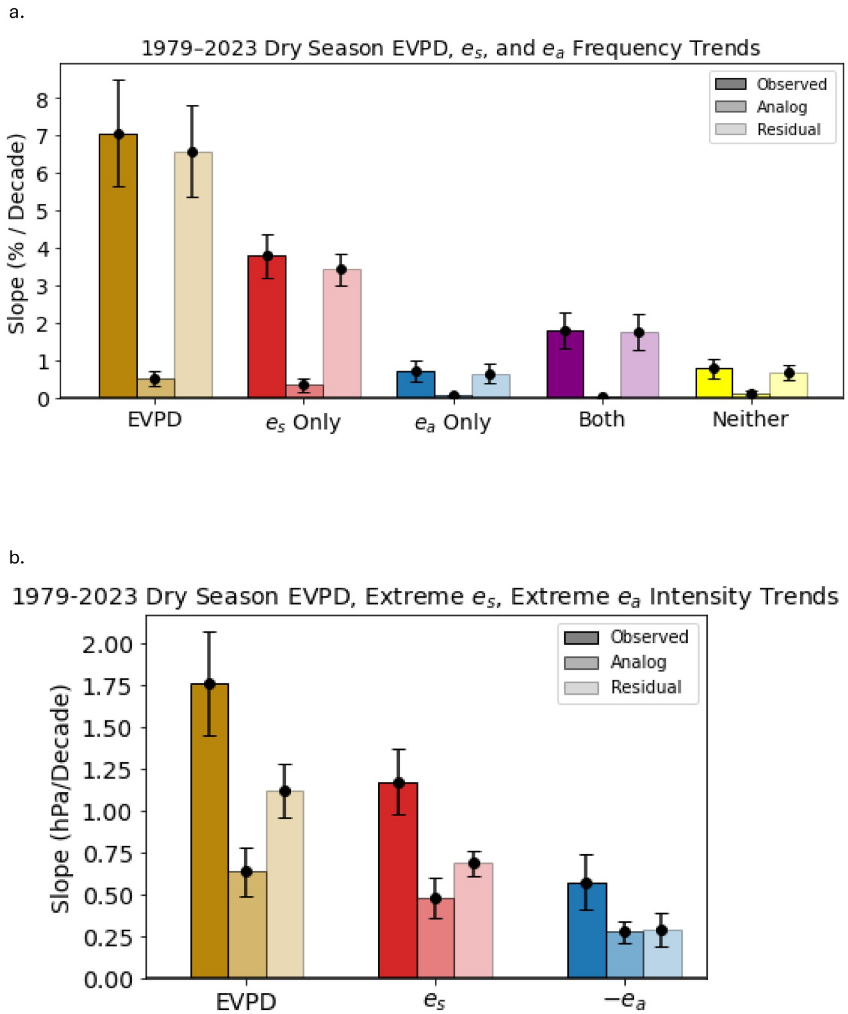

Figure 2. Spatially averaged observed, analog, and residual EVPD, extreme e_s, and extreme e_a frequency (a) and intensity (b) linear regression slopes from 1979 to 2023 during the dry season. Bar plot ranges indicate 95% confidence intervals of the linear regression line. "Both" indicates the frequency trend of simultaneous extreme e_s, and e_a while "neither" indicates the frequency trend of EVPD days with neither extreme e_s, nor extreme e_a.

Figure 2 shows trends in dry season EVPD, e_s, and e_a frequency and intensity, during 1979–2023, as well as each of their analog and residual counterparts, spatially averaged over the Southern Amazon domain. EVPD frequency has increased at 7 ± 1.4% (11 ± 2 dry season days) per decade from 1979 to 2023 (Figure 2a), which is equivalent to 1.1 ± 0.2σ per decade (σ is the standard deviation of EVPD frequency for the reference period of 1979–2000, which is 6.2%). This trend leads to an increase in EVPD frequency of 31.8 ± 6.3% (49 ± 10 dry season days, 5.1 ± 1σ) during 1979–2023, which exceeds the range of natural climate variability. The analog EVPD frequency trend is 0.5 ± 0.2% (0.8 ± 0.3 dry season days) per decade. The relative contribution of natural climate variability to increases in EVPD frequency (the ratio of the analog vs. observed EVPD frequency trend) is only 7% (4%–13% uncertainty estimate), with the remaining 93% (87%–96% uncertainty estimate) of the observed EVPD frequency trend attributable to climate change.

Figure 2a shows that extreme e_s frequency has increased at 3.8 ± 0.6% (6 ± 1 dry season days) per decade during the days when the EVPD threshold was exceeded, accounting for 54% of the observed trends in EVPD frequency. In contrast, the increases in extreme e_a frequency (0.7 ± 0.3% or 1 ± 0.5 dry season days per decade) contributed only 10% to the increases in EVPD frequency. The sum of the extreme e_s and extreme e_a frequency trends is less than the EVPD frequency trend because both extreme e_s and e_a can occur simultaneously during the days when the EVPD threshold was exceeded, and there are days when neither e_s nor e_a exceeds its extreme threshold, but the

EVPD threshold is still exceeded when their combined effects are considered. The trend in the co-occurrence of extreme e_s and e_a frequency is 1.8 ± 0.5% (3 ± 0.8 dry season days) per decade (26% contribution to EVPD frequency trends), and the trend in the remaining EVPD days with neither extreme e_s nor extreme e_a is 0.8 ± 0.3% (1 ± 0.5 dry season days) per decade (11% contribution to EVPD frequency trends).

The analog extreme e_s frequency trend of 0.4 ± 0.2% (0.6 ± 0.3 dry season days) per decade suggests that natural climate variability explains only 11% of the observed increases in extreme e_s frequency. Similarly, the analog extreme e_a trend of 0.08 ± 0.05% (0.1 ± 0.1 dry season days) per decade only explains 3% of the observed extreme e_a frequency trend. Thus, the remaining 89% and 97% of the increases in extreme e_s and e_a frequencies, respectively, are attributable to climate change. Similarly low percentages are seen in the analog trends and relative contributions for the co-occurrence of e_s and e_a extremes and for the EVPD occurrences without extreme e_s or e_a.

Averaged in the Southern Amazon domain, from 1979 to 2000, the average dry-season EVPD intensity was approximately 18 hPa, with lower values in the northwest and higher values in the southeast portion (Figures S4a and S4b in Supporting Information S1). EVPD intensity (Figure 2b) has increased at 1.8 ± 0.3 hPa per decade (8.1 ± 1.4 hPa total from 1979 to 2023), which is 38% greater than that of mean VPD (1.3 ± 0.3 hPa per decade, or (5.8 ± 1.4 hPa total from 1979 to 2023)). The analog EVPD intensity trend of 0.65 ± 0.15 hPa per decade suggests that natural climate variability explains only 36% of the observed increases in EVPD intensity, with the remaining 64% attributable to climate change. 67% of the increases in EVPD intensity are due to increases in extreme e_s intensity at 1.2 ± 0.2 hPa per decade, with the remaining 33% due to decreases in extreme e_a intensity at −0.6 ± 0.2 hPa per decade.

We note that the previous results regarding EVPD may not sufficiently show localized EVPD trends. Grouping areas with vastly different tree cover percentage (Figure S2 in Supporting Information S1) can mask the effects of land-use changes and land-atmosphere feedbacks between forested and deforested areas on EVPD trends. While the exact magnitudes of the EVPD trends differ between forested and deforested areas, the overall conclusions regarding these trends do not change (Figure S5 in Supporting Information S1). Thus, the domain-averaged results are still a good general representation of EVPD trends in the Southern Amazon overall.

To evaluate how the increases in VPD have made atmospheric conditions more conducive to increased wildfire risks and ecosystem water stress, we assess how the frequency of VPD exceeding 25 hPa has changed over time in the Southern Amazon domain. This threshold has been generally associated with increased wildfire risks and greater vegetation water stress over tropical moist biomes such as the Southern Amazon (Clarke et al., 2022; Grossiord et al., 2020), though it does not account for spatial heterogeneity at the local scale. Figure 3a shows that, during 1979–2000, in 89% of the Southern Amazon domain, less than 5% of dry season days experienced VPD exceeding 25 hPa. By 2001–2023, however, in more than half (53%) of the Southern Amazon domain, VPD exceeded 25 hPa during more than 5% of dry season days (Figure 3b). Specifically, VPD exceeded this threshold on 5%–25% of dry season days in the north-central Southern Amazon, where 1979–2000 mean VPD intensity is lower than 12 hPa (Figure S4a in Supporting Information S1). These results suggest increases in the frequency of atmospheric conditions favorable for greater wildfire risks and vegetation water stress in the Southern Amazon, especially in the north-central areas. We note that because of the large spatial heterogeneity in tree cover percentage in different parts of the Southern Amazon (Figure S2 in Supporting Information S1), areas such as the Brazilian Highlands (with Cerrado savanna woodlands) may respond differently to VPD exceeding 25 hPa than more forested areas do, and the use of a singular VPD threshold across the whole region can mask these localized effects. However, these percentages increase in both forested and deforested areas within the domain, indicating broader increases in the likelihoods of atmospheric conditions conducive to greater wildfire risks and vegetation water stress regardless of where they occur within the Southern Amazon.

3.2. Future EVPD Trends

Given that increases in both EVPD frequency and intensity in recent decades are primarily driven by anthropogenic forcing, it is critical to assess how both EVPD metrics will change in the future. To do so, we analyze the projections of climate models from the Coupled Model Intercomparison Project Phase 6 (CMIP6) under two Shared Socioeconomic Pathway (SSP) emissions scenarios (Eyring et al., 2016).

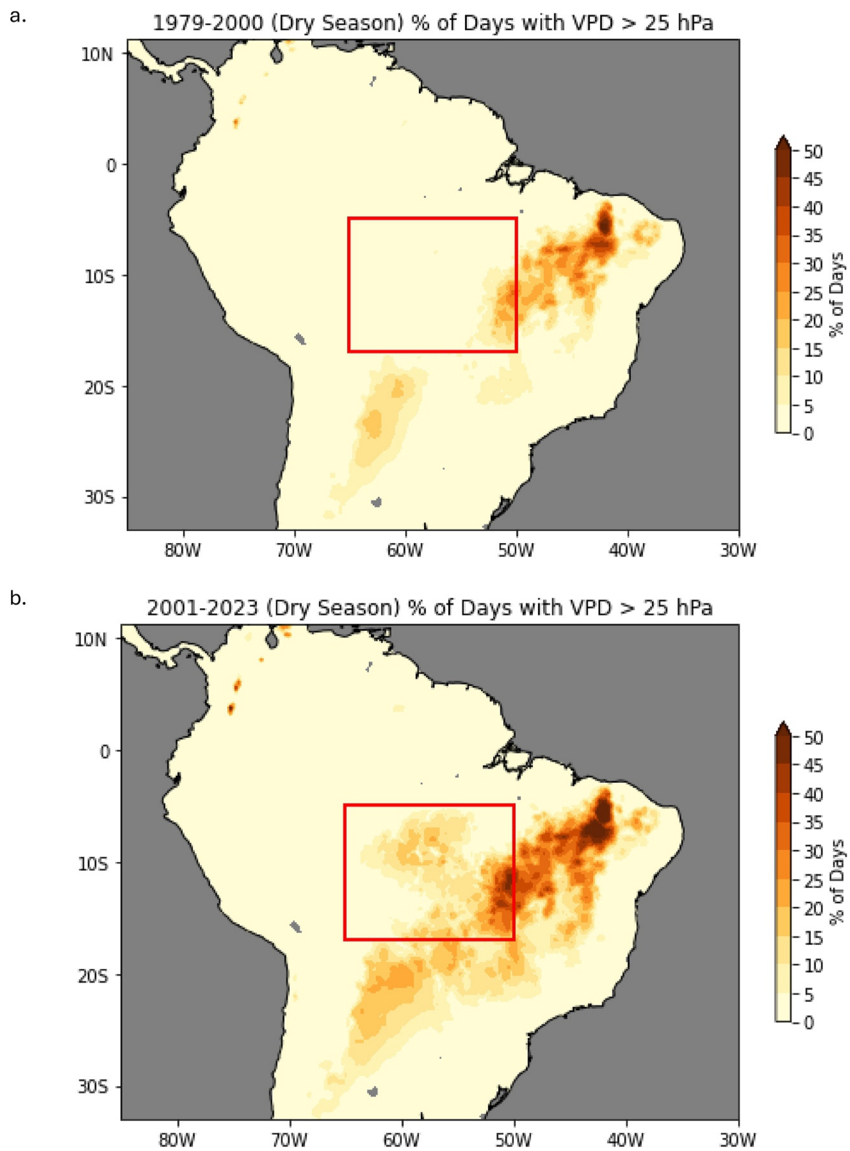

Figure 3. Average percentage of days during the dry season across tropical South America with VPD greater than 25 hPa from (a) 1979–2000, and (b) 2001–2023.

Figure 4a shows that the observed EVPD intensity trend falls within the 5%–95% range of the historical CMIP6 ensemble simulations and future projections for most years from 1979 to 2023. The historical ensemble-mean modeled EVPD intensity trend is 1.2 ± 0.3 hPa per decade from 1979 to 2014, which agrees with the residual EVPD intensity trend for the same time period (1.1 ± 0.2 hPa per decade), indicating that CMIP6 models likely realistically simulate the primary impact of anthropogenic forcing on observed EVPD intensity trends. For extreme e_s intensity (Figure S6a in Supporting Information S1), the CMIP6 historical simulations ensemble mean trend is 1.1 ± 0.1 hPa per decade, somewhat larger than the residual e_s intensity trend of 0.7 ± 0.1 hPa per decade from 1979 to 2014. This discrepancy is likely due to warm surface temperature biases over South America (Bazzanela et al., 2023) and potential underestimations of anthropogenically forced surface temperature increases in the residual e_s trend (Materials and Methods). The extreme e_a intensity trends simulated by the CMIP6 historical simulations (Figure S6b in Supporting Information S1) show a weak drying trend of −0.2 ± 0.1 hPa per decade, which matches the residual extreme e_a intensity trend of −0.2 ± 0.1 hPa per decade. Despite the aforementioned overestimates of the anthropogenically forced extreme e_s intensity trends, the sum of extreme e_s and e_a intensity trends matches the EVPD intensity trends within the uncertainty range for the ensemble mean of

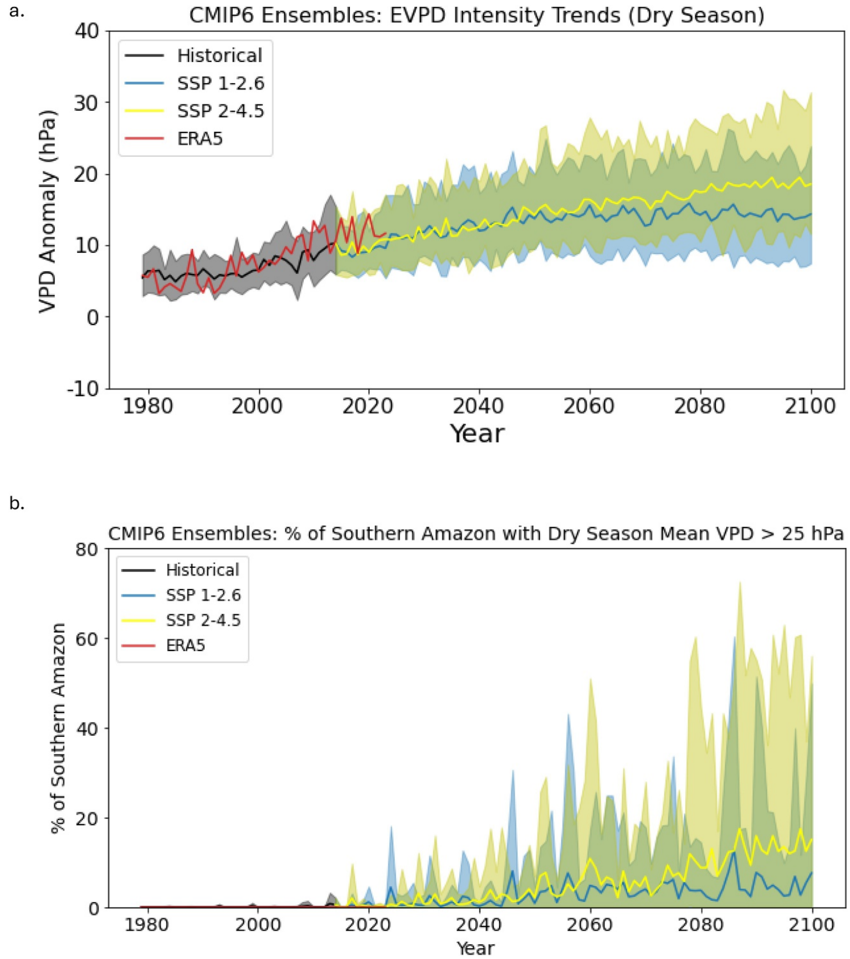

Figure 4. (a) CMIP6 ensemble-averaged EVPD anomalies and (b) CMIP6 ensemble-averaged % of area in the Southern Amazon with dry-season average VPD greater than 25 hPa. Historical simulations from 1979 to 2014 and future simulations from 2015 to 2100 under SSP 1–2.6 and 2–4.5 experiments. Shaded areas indicate the range of the middle 5%–95% of the ensembles.

historical simulations of CMIP6. Thus, these simulations have generally captured the anthropogenically forced EVPD intensity trend and its main drivers as suggested by observations.

In the future, Figure 4a shows that, under the SSP 1-2.6 scenario, ensemble-averaged EVPD intensity is projected to increase to approximately 14 hPa (7.3σ) above the 1979–2000 means by the 2050s before plateauing throughout the remainder of the century, and 90% of the ensembles show EVPD intensity values between 7 and 21 hPa (3.6–10.8σ) at that time. Under the SSP 2-4.5 scenario, EVPD intensity is projected to rise to about 15 hPa (7.6σ) above the climatological values by the 2050s, and to 18 hPa (9.3σ) above the climatological values by 2100. 90% of the SSP 2-4.5 ensembles show EVPD intensity between 9 and 21 hPa (4.6–10.8σ) by 2050 and 13–29 hPa (6.7–14.8σ) by 2100. These projected EVPD intensity increases are almost entirely due to increases in extreme surface temperatures (Figure 4a, Figure S6 in Supporting Information S1) and far exceed the range of 1979–2000 natural climate variability (3σ).

To assess the potential impact of future EVPD increases on atmospheric conditions associated with negative impacts to the Amazonian ecosystem, we evaluate the percentage of grid points within the Southern Amazon where dry season mean VPD is projected to exceed 25 hPa under the SSP scenarios discussed above (Figure 4b). Under the SSP 1–2.6 scenario, the CMIP6 ensemble mean projects that by mid-century (2040–2060), up to 8 ± 5% of the Southern Amazon is most likely to experience dry season mean VPD above 25 hPa (Figure 4b). This percentage further increases to up to 13 ± 7% by the end of the century (2080–2100). Under the SSP 2-4.5

 10.1029/2026GL123139

scenario, the ensemble mean indicates that dry season mean VPD will exceed 25 hPa in up to 8 ± 5% of the Southern Amazon by mid-century and up to 17 ± 7% of locations by the end of the century.

4. Discussion

Our study shows that the increases in EVPD frequency and intensity are greater in more humid and forested areas in the northwest Southern Amazon than in drier and less forested areas in the southeast Southern Amazon (Figure 1, Figure S2 in Supporting Information S1). This is mostly due to more significant increases in anthropogenically forced extreme surface temperatures in the former than in the latter. This result is generally consistent with greater increases in mean VPD in the equatorial Amazon than in the Southern Amazon (Jain et al., 2021), and a secondary influence of deforestation on the changes in dry season mean VPD (Barkhordarian et al., 2019).

Our observation-based attribution provides critical validation of CMIP6 climate model historical simulations and supports the credibility of future projections. These results underscore that future increases in EVPD frequency and intensity will be primarily governed by the trajectory of greenhouse gas emissions.

Current global greenhouse gas emissions are generally aligned with the "middle-of-the-road" emissions scenario (SSP 2–4.5) (Calvin et al., 2023). If this trajectory continues, the ensemble mean of CMIP6 models project that dry season mean VPD will exceed 25 hPa over 22% of forested areas (where tree cover >50%) in the Southern Amazon by 2100. When combined with additional stressors such as the lengthening dry season (Fu et al., 2013; Marengo et al., 2024), more frequent and intense droughts, and land-use changes (Marengo et al., 2018), these changes may render future climates unsustainable in areas beyond the directly impacted regions (Nobre et al., 2016; Salazar & Nobre, 2010). In contrast, if society collectively reduces greenhouse gas emissions according to the "sustainability" scenario (SSP 1–2.6), we can limit the areas where dry season mean VPD exceeds 25 hPa to less than 15% of the forested areas in the Southern Amazon and substantially reduce the impacts of temperature-driven high VPD.

This study only addresses changes in atmospheric moisture demand, as represented by the VPD, over the Southern Amazon. How such changes would affect the evaporative loss of plants and soil moisture is still debated (Novick et al., 2016; Vargas Zeppetello et al., 2023) and beyond the scope of this study.

Previous studies attribute long-term residual VPD trends to anthropogenic climate change (Zhuang et al., 2021). This is supported by the results of Figure S7 in Supporting Information S1. CMIP6 natural simulations account for natural forcings (e.g., solar, volcanic) only, and the differences in EVPD trends between the CMIP6 historical and natural simulations are attributable primarily to anthropogenic forcing. Given that the CMIP6 historical minus natural EVPD frequency and intensity trends align with those of the ERA5 residuals, this supports attributing the residual between the ERA5 observed and analog EVPD trends primarily to anthropogenic forcing.

There is considerable uncertainty in the analog-based attribution analysis. The analog EVPD does not fully account for the impacts of land surface, soil moisture, vegetation, and cloud radiation feedbacks on EVPD, which may vary under the same atmospheric circulation patterns (at the local scale in particular). This limitation would likely underestimate the EVPD associated with natural climate variability. Additionally, the analog could also overestimate the EVPD variation associated with natural climate variability by assuming all the changes of atmospheric circulation patterns are due to natural climate variability. Because of large uncertainties in quantifying these effects in literature, especially over data-limited regions such as the Amazon, we do not know the extent to which they can compensate each other. Therefore, further work is needed to disentangle the effects of non-linear thermodynamic feedbacks and climate change impacts on large-scale atmospheric circulation changes.

The overall conclusions regarding EVPD frequency and intensity trends are not sensitive to the choice of the reference period. Figure S8 in Supporting Information S1 shows that the 95% confidence intervals of the observed and analog EVPD time series trends for different reference periods overlap and are considered statistically indifferent. Additionally, the results are not sensitive to the number of analogs used. While the analog trends vary by as much as 5% between different numbers of analogs used (Table S4 in Supporting Information S1), they still lead to the same overall conclusions regarding EVPD frequency and intensity.

Conflict of Interest

The authors declare no conflicts of interest relevant to this study.

Availability Statement

All ERA5 data used in this study are available at the Copernicus Climate Data Store via https://doi.org/10.24381/cds.adbb2d47 under a CC-BY license (Copernicus Climate Change Service, Climate Data Store, 2023).

The list of CMIP6 models used is available in Tables S1 and S2 in Supporting Information S1. All CMIP6 data used in this study are available at the Earth System Grid Federation Nodes via https://esgf-node.ornl.gov/search/cmip6 under a CC-BY license (Eyring et al., 2016).

Figures were made with Matplotlib version 3.5.1 (Hunter, 2007), available under a Matplotlib license at https://matplotlib.org/stable/project/license.html.

Acknowledgments

This study was supported by the National Science Foundation grants #1917781 and #2214697. We thank the European Center for Medium-Range Weather Forecasts (ECMWF), who provided the relevant reanalysis data; the World Climate Research Programme (WCRP) and Lawrence Livermore National Laboratory (LLNL), who provided the relevant CMIP6 model data; and the Atmospheric and Oceanic Sciences (AOS) Department at the University of California Los Angeles (UCLA), who provided the computing resources.

References

Barkhordarian, A., Saatchi, S. S., Behrangi, A., Loikith, P. C., & Mechoso, C. R. (2019). A recent systematic increase in vapor pressure deficit over tropical South America. *Scientific Reports*, *9*(1), 15331. https://doi.org/10.1038/s41598-019-51857-8

Basso, L. S., Wilson, C., Chipperfield, M. P., Tejada, G., Cassol, H. L. G., Arai, E., et al. (2023). Atmospheric co2 inversion reveals the Amazon as a minor carbon source caused by fire emissions, with forest uptake offsetting about half of these emissions. *Atmospheric Chemistry and Physics*, *23*(17), 9685–9723. https://doi.org/10.5194/acp-23-9685-2023

Bazzanela, A. C., Dereczynski, C., Luiz-Silva, W., & Regoto, P. (2023). Performance of CMIP6 models over South America. *Climate Dynamics*, *62*(2), 1501–1516. https://doi.org/10.1007/s00382-023-06979-1

Calvin, K., Dasgupta, D., Krinner, G., Mukherji, A., Thorne, P. W., Trisos, C., et al. (Eds.), Contribution of working groups I, II and III to the sixth assessment report of the intergovernmental panel on climate change [core writing team, H. Lee and J. Romero (eds.). IPCC. https://doi.org/10.59327/ipcc/ar6-9789291691647

Clarke, H., Nolan, R. H., De Dios, V. R., Bradstock, R., Griebel, A., Khanal, S., & Boer, M. M. (2022). Forest fire threatens global carbon sinks and population centres under rising atmospheric water demand. *Nature Communications*, *13*(1), 7161. https://doi.org/10.1038/s41467-022-34966-3

Copernicus Climate Change Service, & Climate, D. S. (2023). Era5 hourly data on single levels from 1940 to present [Dataset]. *Copernicus Climate Change Service (C3S) Climate Data Store (CDS)*. https://doi.org/10.24381/cds.adbb2d47

Crivelari-Costa, P. M., Lima, M., La Scala, N., Jr., Rossi, F. S., Della-Silva, J. L., Dalagnol, R., et al. (2023). Changes in carbon dioxide balance associated with land use and land cover in Brazilian legal amazon based on remotely sensed imagery. *Remote Sensing*, *15*(11), 2780. https://doi.org/10.3390/rs15112780

Deser, C., Knutti, R., Solomon, S., & Phillips, A. S. (2012). Communication of the role of natural variability in future North American climate. *Nature Climate Change*, *2*(11), 775–779. https://doi.org/10.1038/nclimate1562

Eyring, V., Bony, S., Meehl, G. A., Senior, C. A., Stevens, B., Stouffer, R. J., & Taylor, K. E. (2016). Overview of the coupled model intercomparison project phase 6 (CMIP6) experimental design and organization. *Geoscientific Model Development*, *9*(5), 1937–1958. https://doi.org/10.5194/gmd-9-1937-2016

Flores, B. M., Montoya, E., Sakschewski, B., Nascimento, N., Staal, A., Betts, R. A., et al. (2024). Critical transitions in the Amazon forest system. *Nature*, *626*(7999), 555–564. https://doi.org/10.1038/s41586-023-06970-0

Fu, R., Yin, L., Li, W., Arias, P. A., Dickinson, R. E., Huang, L., et al. (2013). Increased dry-season length over southern Amazonia in recent decades and its implication for future climate projection. *Proceedings of the National Academy of Sciences*, *110*(45), 18110–18115. https://doi.org/10.1073/pnas.1302584110

Gatti, L. V., Basso, L. S., Miller, J. B., Gloor, M., Domingues, L. G., Cassol, H. L. G., et al. (2021). Amazonia as a carbon source linked to deforestation and climate change. *Nature*, *595*(7867), 388–393. https://doi.org/10.1038/s41586-021-03629-6

Grossiord, C., Buckley, T. N., Cernusak, L. A., Novick, K. A., Poulter, B., Siegwolf, R. T. W., et al. (2020). Plant responses to rising vapor pressure deficit. *New Phytologist*, *226*(6), 1550–1566. https://doi.org/10.1111/nph.16485

Hawkins, E., & Sutton, R. (2012). Time of emergence of climate signals. *Geophysical Research Letters*, *39*(1). https://doi.org/10.1029/2011gl050087

Hersbach, H., Bell, B., Berrisford, P., Hirahara, S., Horányi, A., Muñoz-Sabater, J., et al. (2020). The ERA5 global reanalysis. *Quarterly Journal of the Royal Meteorological Society*, *146*(730), 1999–2049. https://doi.org/10.1002/qj.3803

Hubau, W., Lewis, S. L., Phillips, O. L., Affum-Baffoe, K., Beeckman, H., Cuní-Sanchez, A., et al. (2020). Asynchronous carbon sink saturation in African and Amazonian tropical forests. *Nature*, *579*(7797), 80–87. https://doi.org/10.1038/s41586-020-2035-0

Hunter, J. D. (2007). Matplotlib: A 2D graphics environment [Software]. *Computing in Science & Engineering*, *9*(3), 90–95. https://doi.org/10.1109/MCSE.2007.55

Jain, P., Castellanos-Acuna, D., Coogan, S. C. P., Abatzoglou, J. T., & Flannigan, M. D. (2021). Observed increases in extreme fire weather driven by atmospheric humidity and temperature. *Nature Climate Change*, *12*(1), 63–70. https://doi.org/10.1038/s41558-021-01224-1

Joetzjer, E., Douville, H., Delire, C., & Ciais, P. (2013). Present-day and future Amazonian precipitation in global climate models: CMIP5 versus CMIP3. *Climate Dynamics*, *41*(11–12), 2921–2936. https://doi.org/10.1007/s00382-012-1644-1

Lehner, F., Deser, C., Simpson, I. R., & Terray, L. (2018). Attributing the U.S. Southwest's recent shift into drier conditions. *Geophysical Research Letters*, *45*(12), 6251–6261. https://doi.org/10.1029/2018gl078312

Leite-Filho, A. T., Soares-Filho, B. S., Davis, J. L., Abrahão, G. M., & Börner, J. (2021). Deforestation reduces rainfall and agricultural revenues in the Brazilian Amazon. *Nature Communications*, *12*(1), 2591. https://doi.org/10.1038/s41467-021-22840-7

Li, W., & Fu, R. (2006). Influence of cold air intrusions on the wet season onset over Amazonia. *Journal of Climate*, *19*(2), 257–275. https://doi.org/10.1175/jcli3614.1

Marengo, J. A., Cunha, A. P., Espinoza, J.-C., Fu, R., Schöngart, J., Jimenez, J. C., et al. (2024). The drought of Amazonia in 2023-2024. *American Journal of Climate Change*, *13*(3), 567–597. https://doi.org/10.4236/ajcc.2024.133026
Marengo, J. A., Souza, C. M., Thonicke, K., Burton, C., Halladay, K., Betts, R. A., et al. (2018). Changes in climate and land use over the Amazon region: Current and future variability and trends. *Frontiers in Earth Science*, *6*, 228. https://doi.org/10.3389/feart.2018.00228
Nobre, C. A., Sampaio, G., Borma, L. S., Castilla-Rubio, J. C., Silva, J. S., & Cardoso, M. (2016). Land-use and climate change risks in the Amazon and the need of a novel sustainable development paradigm. *Proceedings of the National Academy of Sciences*, *113*(39), 10759–10768. https://doi.org/10.1073/pnas.1605516113
Novick, K. A., Ficklin, D. L., Grossiord, C., Konings, A. G., Martínez-Vilalta, J., Sadok, W., et al. (2024). The impacts of rising vapour pressure deficit in natural and managed ecosystems. *Plant, Cell and Environment*, *47*(9), 3561–3589. https://doi.org/10.1111/pce.14846
Novick, K. A., Ficklin, D. L., Stoy, P. C., Williams, C. A., Bohrer, G., Oishi, A. C., et al. (2016). The increasing importance of atmospheric demand for ecosystem water and carbon fluxes. *Nature Climate Change*, *6*(11), 1023–1027. https://doi.org/10.1038/nclimate3114
Salazar, L. F., & Nobre, C. A. (2010). Climate change and thresholds of biome shifts in Amazonia. *Geophysical Research Letters*, *37*(17). https://doi.org/10.1029/2010gl043538
Sancho-Knapik, D., Mendoza-Herrer, s., Alonso-Forn, D., Saz, M. N., Martín-Sánchez, R., dos Santos Silva, J. V., et al. (2022). Vapor pressure deficit constrains transpiration and photosynthesis in holm oak: A comparison of three methods during summer drought. *Agricultural and Forest Meteorology*, *327*, 109218. https://doi.org/10.1016/j.agrformet.2022.109218
Stouffer, R. J., Eyring, V., Meehl, G. A., Bony, S., Senior, C., Stevens, B., & Taylor, K. E. (2017). CMIP5 scientific gaps and recommendations for CMIP6. *Bulletin of the American Meteorological Society*, *98*(1), 95–105. https://doi.org/10.1175/bams-d-15-00013.1
Vargas Zeppetello, L. R., McColl, K. A., Bernau, J. A., Bowen, B. B., Tang, L. I., Holbrook, N. M., et al. (2023). Apparent surface conductance sensitivity to vapour pressure deficit in the absence of plants. *Nature Water*, *1*(11), 941–951. https://doi.org/10.1038/s44221-023-00147-9
Will, R. E., Wilson, S. M., Zou, C. B., & Hennessey, T. C. (2013). Increased vapor pressure deficit due to higher temperature leads to greater transpiration and faster mortality during drought for tree seedlings common to the forest–grassland ecotone. *New Phytologist*, *200*(2), 366–374. https://doi.org/10.1111/nph.12321
Yang, Y., Saatchi, S. S., Xu, L., Yu, Y., Choi, S., Phillips, N., et al. (2018). Post-drought decline of the Amazon carbon sink. *Nature Communications*, *9*(1), 3172. https://doi.org/10.1038/s41467-018-05668-6
Yin, L., Fu, R., Zhang, Y., Arias, P. A., Fernando, D. N., Li, W., et al. (2014). What controls the interannual variation of the wet season onsets over the Amazon? *Journal of Geophysical Research: Atmospheres*, *119*(5), 2314–2328. https://doi.org/10.1002/2013jd021349
Yiou, P. (2014). AnaWEGE: A weather generator based on analogues of atmospheric circulation. *Geoscientific Model Development*, *7*(2), 531–543. https://doi.org/10.5194/gmd-7-531-2014
Yiou, P., Vautard, R., Naveau, P., & Cassou, C. (2007). Inconsistency between atmospheric dynamics and temperatures during the exceptional 2006/2007 fall/winter and recent warming in Europe. *Geophysical Research Letters*, *34*(21). https://doi.org/10.1029/2007gl031981
Zhuang, Y., Fu, R., Santer, B. D., Dickinson, R. E., & Hall, A. (2021). Quantifying contributions of natural variability and anthropogenic forcings on increased fire weather risk over the western United States. *Proceedings of the National Academy of Sciences*, *118*(45), e2111875118. https://doi.org/10.1073/pnas.2111875118

References From the Supporting Information

Alduchov, O. A., & Eskridge, R. E. (1996). Improved magnus form approximation of saturation vapor pressure. *Journal of Applied Meteorology*, *35*(4), 601–609. https://doi.org/10.1175/1520-0450(1996)035⟨0601:imfaos⟩2.0.co;2
Cannon, A. J., Sobie, S. R., & Murdock, T. Q. (2015). Bias correction of GCM precipitation by quantile mapping: How well do methods preserve changes in quantiles and extremes? *Journal of Climate*, *28*(17), 6938–6959. https://doi.org/10.1175/jcli-d-14-00754.1
Draper, N. R., & Smith, H. (1998). *Applied regression analysis*. Wiley. https://doi.org/10.1002/9781118625590
Durbin, J., & Watson, G. S. (1950). Testing for serial correlation in least squares regression. *i. Biometrika*, *37*(3–4), 409–428. https://doi.org/10.1093/biomet/37.3-4.409
Lehner, F., Nadeem, I., & Formayer, H. (2023). Evaluating skills and issues of quantile-based bias adjustment for climate change scenarios. *Advances in Statistical Climatology, Meteorology and Oceanography*, *9*(1), 29–44. https://doi.org/10.5194/ascmo-9-29-2023
Stott, P. A., Christidis, N., Otto, F. E. L., Sun, Y., Vanderlinden, J.-P., van Oldenborgh, G. J., et al. (2015). Attribution of extreme weather and climate-related events. *WIREs Climate Change*, *7*(1), 23–41. https://doi.org/10.1002/wcc.380
Xavier, A. C. F., Martins, L. L., Rudke, A. P., de Morais, M. V. B., Martins, J. A., & Blain, G. C. (2021). Evaluation of quantile delta mapping as a bias-correction method in maximum rainfall dataset from downscaled models in São Paulo state (Brazil). *International Journal of Climatology*, *42*(1), 175–190. https://doi.org/10.1002/joc.7238